Effect of wave frequency and directional spread on shoreline runup

R. T. Guza[1] and Falk Feddersen[1]

Received 6 April 2012; revised 10 May 2012; accepted 11 May 2012; published 7 June 2012.

[1] Wave breaking across the surf zone elevates the mean water level at the shoreline (setup), and drives fluctuations about the mean (runup). Runup often is divided into sea-swell (0.04–0.3 Hz) and lower frequency infragravity (0.00–0.04 Hz) components. With energetic incident waves, runup is dominated by infragravity frequencies, and total water levels (combined setup and runup) can exceed 3 m, significantly contributing to coastal flooding and erosion. Setup and runup observations on sandy beaches are scattered about empirical parameterizations based on near-shoreline beach slope and deep water wave height and wavelength. Accurate parameterizations are needed to determine flooding and erosion risk to coastal ecosystems and communities. Here, numerical simulations with the Boussinesq wave model funwaveC are shown to statistically reproduce typical empirical setup and runup parameterizations. Furthermore, the model infragravity runup $R_s^{(ig)}$ strongly depends on the incident wave directional and frequency spread (about the mean direction and peak frequency). Realistic directional spread variations change $R_s^{(ig)}$ equivalent to a factor of two variation in incident wave height. The modeled $R_s^{(ig)}$ is shown to vary systematically with a new, non-dimensional spreading parameter that involves peak frequency, frequency spread, and directional spread. This suggests a new parameterization for $R_s^{(ig)}$ potentially useful to predict coastal flooding and erosion. **Citation:** Guza, R. T., and F. Feddersen (2012), Effect of wave frequency and directional spread on shoreline runup, *Geophys. Res. Lett.*, *39*, L11607, doi:10.1029/2012GL051959.

1. Introduction

[2] Waves incident to a beach elevate the shoreline mean water level (setup, $\bar{R}$) and drive fluctuations about the mean (runup). Energetic waves can elevate total water level (combined setup and runup) by as much as 3 m [*Stockdon et al.*, 2006]. Empirical parameterizations of wave-induced setup $\bar{R}$ (super-elevation of the mean shoreline location) and runup (fluctuations of the waterline about the mean) are often used to predict coastal flooding and erosion [*Ruggiero et al.*, 2001; *Anselme et al.*, 2011; *Revell et al.*, 2011]. Runup often is divided into sea-swell (0.04–0.3 Hz, $R_s^{(ss)}$) and infragravity (0.004–0.04 Hz, $R_s^{(ig)}$) frequency bands, with significant runup elevation R_s defined as 4σ, where σ^2 is the vertical runup variance in that band. During energetic wave events, $R_s^{(ig)}$ dominates runup on dissipative beaches [*Guza and Thornton*, 1982]. Thus accurately parameterizing $R_s^{(ig)}$ is critical to predicting wave-driven coastal flooding and its impacts on coastal ecosystems and communities.

[3] Many empirical parameterizations relate $\bar{R}$, $R_s^{(ss)}$, or $R_s^{(ig)}$ to incident wave conditions and beach slope β [*Holman*, 1986; *Ruessink et al.*, 1998; *Stockdon et al.*, 2006; *Senechal et al.*, 2011; and others], typically proportional to $(H_{s,0}L_0)^{1/2}$ or $\beta(H_{s,0}L_0)^{1/2}$ where L_0 is the incident deep water wavelength based on peak (or mean) frequency f_p ($L_0 = (2\pi g)f_p^{-2}$), and $H_{s,0}$ is the deep-water significant wave height (i.e., unshoaled to deep water on plane parallel bathymetry). On natural, non-planar beaches, β is often approximated as the linear beach slope near the waterline [e.g., *Stockdon et al.*, 2006]. Although empirical parameterization for $R_s^{(ig)}$ using $(H_{s,0}L_0)^{1/2}$ have significant skill ($r^2 \approx 0.65$ for $R_s^{(ig)} \propto (H_{s,0}L_0)^{1/2}$) [e.g., *Stockdon et al.*, 2006], scatter can be significant. The incident sea-swell directional spectrum, which nonlinearly forces infragravity waves in shallow water, depends not only on $H_{s,0}$ and f_p, but also has frequency spread (f_s) about f_p and directional spread (σ_θ) [*Kuik et al.*, 1988] about the mean angle (assumed zero here), The effect of variable f_d and σ_θ on infragravity runup $R_s^{(ig)}$ is explored here using the Boussinesq wave model funwaveC on a planar beach.

[4] The model (section 2) is shown to reproduce the dependence on $(H_{s,0}L_0)^{1/2}$ and $\beta(H_{s,0}L_0)^{1/2}$ (section 3.1) of existing setup and runup parameterizations, suggesting that it can be used to model runup quantitatively. The scatter about the $R_s^{(ig)}/(H_{s,0}L_0)^{1/2}$ parameterization depends on f_s and σ_θ (section 3.2). A simple non-dimensional parameter $(f_p / f_s)\sigma_{\theta,0}$ (where $\sigma_{\theta,0}$ is the deep-water σ_θ), based on a nonlinear infragravity wave coupling coefficient, collapses the scatter, suggesting a new $R_s^{(ig)}$ parameterization (section 4).

2. Model Description

[5] The funwaveC model used here, solving the relatively simple [*Nwogu*, 1993] equations, reproduces field observations of surfzone waves and currents [*Feddersen et al.*, 2011] and of tracer dispersion driven by low frequency vortical motions [*Spydell and Feddersen*, 2009; *Clark et al.*, 2011]. Cross- and alongshore grid sizes are 1 m and 1.25 m, respectively. The model bottom stress is quadratic in velocity and for simplicity a spatially uniform drag coefficient $c_d = 0.002$ [*Feddersen et al.*, 2011] is used. Increased c_d in the swash zone [*Puleo and Holland*, 2001], which potentially affects runup, is not included. An eddy viscosity wave breaking method [*Lynett*, 2006] is used with parameter values similar to previous studies [*Feddersen et al.*, 2011]. Runup is implemented using the "thin-layer" method [*Salmon*, 2002] that adds an extra pressure to the equations to keep a minimum fluid thickness d_0 on a sloping shoreline. The d_0 depend on the grid spacing and beach slope, and

[1]Scripps Institution of Oceanography, University of California, San Diego, La Jolla, California, USA.

Corresponding author: F. Feddersen, Scripps Institution of Oceanography, University of California, San Diego, La Jolla, CA 92093-0209 USA. (ffeddersen@ucsd.edu)

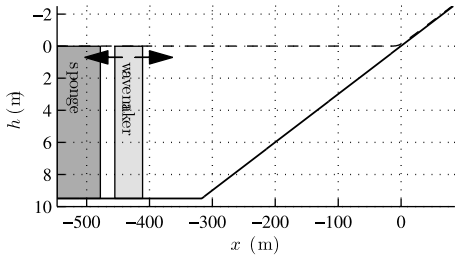

Figure 1. Schematic model planar bathymetry, offshore sponge layer (dark shaded regions), and wavemaker regions versus cross-shore coordinate x, where $x = 0$ m is the still-water shoreline location. The wavemaker (light shaded region) radiates waves onshore and offshore as indicated by the arrows. The dashed curve is the still-water sea-surface. The thin (few cm) layer of water extending up the slope to avoid zero depth is not visible.

ranged between 3–7 cm. Although momentum is not strictly conserved, this method is simple and reproduces analytic solutions [*Carrier and Greenspan*, 1958] for a nonlinear standing wave on a beach [*Salmon*, 2002].

[6] The model bathymetry (Figure 1) has an offshore region of constant depth ($h_0 = 9.5$ m) adjacent to a planar slope region further onshore. The constant depth region length (230–260 m width) contains the wavemaker and an offshore sponge layer (70–100 m width) that absorbs seaward propagating waves. The total cross-shore domain varies between 563–808 m. The alongshore domain L_y, between 1.15–2.25 km, is chosen to allow non-zero incident wave angles as small as 3° (at depth h_0 and peak-frequency f_p) to satisfy the alongshore periodic boundary condition. $R_s^{(ig)}$ is only weakly sensitive to L_y (see Appendix A).

[7] A wavemaker [*Wei et al.*, 1999], located immediately onshore of the offshore sponge layer, generates approximately the target spectrum

$$E(f,\theta) \propto \exp\left[-\left(\frac{f-f_p}{f_s}\right)^2\right] S(\theta) \qquad (1)$$

over the frequency range $f_p \pm f_s$, where f_s is the frequency spread and f_p is the peak frequency. At f_p, $kh < 1$, within the valid range of *Nwogu* [1993]. The symmetric, normally incident directional spectrum $S(\theta)$ has a Gaussian form with width specified by the directional spread σ_θ [*Feddersen et al.*, 2011].

[8] A total of 180 model simulations were performed with independently-varied beach slope β (between 0.02–0.04), incident H_s (between 0.4–2.5 m), peak frequency f_p (between 0.06–0.14 Hz), frequency spreads f_s (between 0.0025–0.02 Hz), and target directional spread σ_θ (between 5–30°). The wave parameters are not independent in naturally occurring waves; low frequency swell is often narrow in frequency and direction, whereas high frequency seas typically have broad spreads. The wave parameter co-variation depends on location and event. The wavemaker only approximately reproduces the target $E(f, \theta)$, and the four incident wave parameters (H_s, f_p, f_s, and σ_θ) are estimated on the flat depth region onshore of the wavemaker with model output. The deep water wave height $H_{s,0}$ and wavelength L_0 are calculated from H_s and f_p. The range of f_p, β and $H_{s,0}$ correspond to Irrabaren numbers $\zeta = \beta(L_0/H_{s,0})^{1/2}$ generally $\zeta < 0.4$, indicating dissipative conditions [*Stockdon et al.*, 2006]. Simulation were sampled for 2400 s after 200 s of model spinup. Alongshore variations in runup statistics were weak.

[9] The model runup toe location $R(t)$, defined as the most shoreward location where fluid thickness $>4d_0$, varied between 9–21 cm above the minimum fluid thickness d_0. If $R(t)$ is too small (relative to d_0), the runup is distorted by the thin film pressure head [*Salmon*, 2002]. Field observed runup statistics depend on the minimum water elevation chosen for the runup toe. Differences in significant runup, between 5 cm and 15 cm elevations, are between 30% and 15% in the sea-swell and infragravity frequency bands, respectively, on a moderately sloped beach with low energy swell waves [*Raubenheimer and Guza*, 1996]. Empirical runup parameterizations were derived primarily with video observations, which corresponds most closely to a 5 cm minimum elevation [*Holland et al.*, 1995]. The effects of different runup toe definitions over a range of wave conditions and beach slopes are unknown, and are neglected here. Model results are not sensitive to variations in toe thickness between $3d_0$–$5d_0$.

[10] Setup $\bar{R}$ is defined as the time- and alongshore average of R. The significant sea-swell $R_s^{(ss)}$ and infragravity $R_s^{(ig)}$ runup elevations are based on the alongshore-averaged runup spectrum integrated over the sea-swell (0.04–0.3 Hz) and infragravity (0.004–0.04 Hz) frequency bands. The upper limit of the infragravity frequency band is typically between 0.04 Hz [e.g., *Herbers et al.*, 1995] and 0.05 Hz [e.g., *Stockdon et al.*, 2006]. Here, 0.04 Hz is used to avoid leaking incident (lowest peak frequency $f_p = 0.06$ Hz) energy into the infragravity band. In analysis of field observations [e.g., *Senechal et al.*, 2011], a lower infragravity-band limit of 0.004 Hz is used to exclude low-frequency motions (e.g., tides), and this limit is used here for consistency. Model results are insensitive to this limit. Similar to field observations [*Holman*, 1986; *Stockdon et al.*, 2006], simulated two-percent runup-exceedences follows $R_{2\%} = 1.05(\bar{R} + R_s/2)$ where R_s includes both sea-swell and infragravity contributions.

3. Results

3.1. Model Comparison With Existing Runup Parameterizations

[11] Model setup and runup statistics $\bar{R}$, $R_s^{(ss)}$, and $R_s^{(ig)}$ fit to parameterizations based on $(H_{s,0}L_0)^{1/2}$ and $\beta(H_{s,0}L_0)^{1/2}$ yield best-fit slopes and squared correlations r^2 (Table 1 and Figure 2) similar to field based results [*Ruessink et al.*, 1998;

Table 1. Regression Statistics Between Runup Quantities and Non-dimensional Parameters $(H_{s,0}L_0)^{1/2}$ and $\beta(H_{s,0}L_0)^{1/2}$[a]

	$(H_{s,0}L_0)^{1/2}$			$\beta(H_{s,0}L_0)^{1/2}$		
	Slope	r^2	rms Error (m)	Slope	r^2	rms Error (m)
$\bar{R}$	0.014	0.58	0.09	0.53	0.71	0.07
$R_s^{(ss)}$	0.021	0.07	0.22	0.82	0.33	0.17
$R_s^{(ig)}$	0.041	0.68	0.21	1.48	0.60	0.23

[a]The slope and root-mean-square error (rms error) are for a fit forced to go through the origin. The squared correlation is r^2. Narrow frequency spreads $f_s = 0.0025$ Hz, that rarely occur in Southern California, are not includedin $R_s^{(ig)}$ statistics.

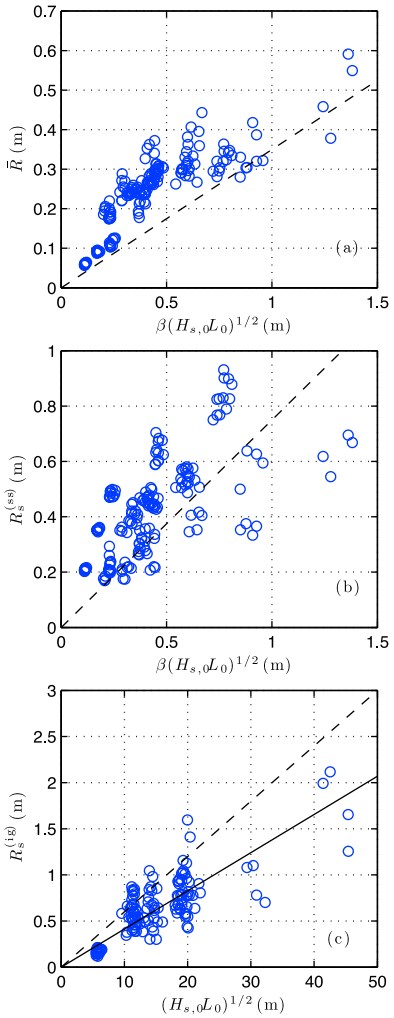

Figure 2. (a) Setup $\bar{R}$ versus $\beta(H_{s,0}L_0)^{1/2}$ for all simulations. The dashed line is the *Stockdon et al.* [2006] slope of 0.35. (b) Sea-swell band ($0.04 < f < 0.3$ Hz) significant runup $R_s^{(ss)}$ versus $\beta(H_{s,0}L_0)^{1/2}$ for all simulations. Dashed line has slope 0.75 [*Stockdon et al.*, 2006]. (c) Infragravity-band ($0.004 < f < 0.04$ Hz) significant runup $R_s^{(ig)}$ versus $(H_{s,0}L_0)^{1/2}$ for simulations with $f_s > 0.0025$ Hz. The dashed and solid lines are the *Stockdon et al.* [2006] (slope of 0.06) and present simulations (slope of 0.041) best-fit slopes.

Stockdon et al., 2006; *Senechal et al.*, 2011]. As with field observations [*Stockdon et al.*, 2006], the setup $\bar{R}$ and the sea-swell band significant runup $R_s^{(ss)}$ had a higher r^2 with $\beta(H_{s,0}L_0)^{1/2}$ than with $(H_{s,0}L_0)^{1/2}$. Although natural beach profiles are not well represented by a single β, the model best-fit regression-slopes using $\beta(H_{s,0}L_0)^{1/2}$ are consistent with those found on natural beaches [*Stockdon et al.*, 2006] (Figures 2a and 2b).

[12] Consistent with prior field observations [*Stockdon et al.*, 2006; *Senechal et al.*, 2011], infragravity-band runup $R_s^{(ig)}$ skill using $(H_{s,0}L_0)^{1/2}$ is higher than with $\beta(H_{s,0}L_0)^{1/2}$ ($r^2 = 0.67$ and 0.60, respectively, for cases with $f_s > 0.0025$ Hz, Table 1 and Figure 2c). The smallest $f_s = 0.0025$ Hz, which rarely occur in Southern California, are excluded from this comparison (Figure 2c) to video-based runup parameterizations. The best-fit slope of 0.041 between $R_s^{(ig)}$ and $(H_{s,0}L_0)^{1/2}$ (solid black line in Figure 2c) is comparable to the *Stockdon et al.* [2006] slope of 0.06 (dashed line in Figure 2c) and the *Senechal et al.* [2011] slope of 0.05 (not shown). The model reproduces the field-based parameterizations (1) of $\bar{R}$, $R_s^{(ss)}$ and $R_s^{(ig)}$, supporting the use of model simulations to explore the neglected effects of frequency (f_s) and directional (σ_θ) spread.

3.2. Frequency and Directional Spread Dependence of $R_s^{(ig)}$

[13] The contributions of f_s and σ_θ to the scatter of $R_s^{(ig)}$ about the parameterizations (Figure 2c) is now explored. At fixed β, f_p and $H_{s,0} \approx 1.25$ m, the normalized infragravity runup $R_s^{(ig)}/(H_{s,0}L_0)^{1/2}$ increases with increasing frequency spread f_s and decreases with increasing directional spread σ_θ (Figure 3a). For Southern California, $f_s = 0.0025$ Hz rarely occurs, and associated $R_s^{(ig)}/(H_{s,0}L_0)^{1/2} \approx 0.02$ are smaller than typically observed. As f_s increases to (more typical for Southern California) 0.01–0.02 Hz, $R_s^{(ig)}/(H_{s,0}L_0)^{1/2} \approx 0.05$ and the sensitivity of $R_s^{(ig)}/(H_{s,0}L_0)^{1/2}$ to f_s decreases. With $f_s \geq 0.01$ Hz, the ratio $R_s^{(ig)}/(H_{s,0}L_0)^{1/2}$ varies by a factor of 1.5 with realistic σ_θ variation from 5° to 30° (Figure 3b). With constant σ_θ, $f_s \geq 0.01$ Hz, and the limited range of moderate β considered (0.02–0.04), the normalized infragravity runup $R_s^{(ig)}/(H_{s,0}L_0)^{1/2}$ does not obviously depend on

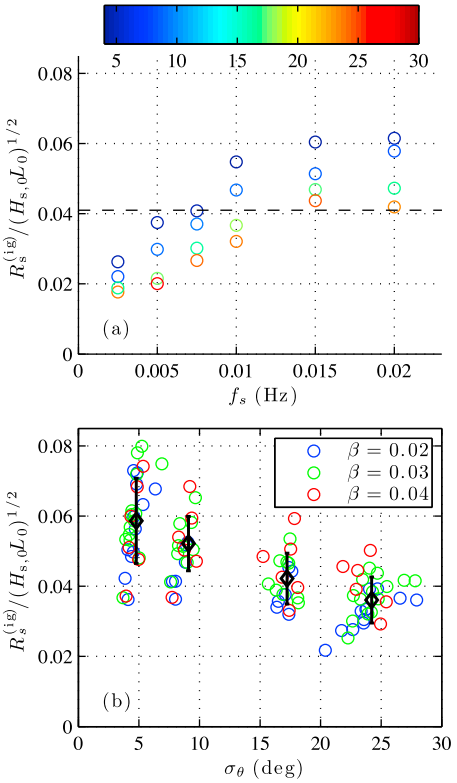

Figure 3. (a) Normalized infragravity-band significant runup height $R_s^{(ig)}/(H_{s,0}L_0)^{1/2}$ versus frequency spread f_s and σ_θ (color scale, in degrees) for simulations with constant $f_s = 0.1$ Hz, $\beta = 0.03$, and $H_{s,0} \approx 1.25$ m. The dashed line corresponds to the best-fit slope 0.041 (Figure 2c). (b) $R_s^{(ig)}/(H_{s,0}L_0)^{1/2}$ versus directional spread σ_θ with three beach slopes β (see legend). At each σ_θ and β, the same set of f_p and $H_{s,0}$ with $f_s \geq 0.01$ Hz are shown to focus on the effects of varying β and σ_θ. The binned-means and ± standard deviation are given by the black diamonds and vertical bars.

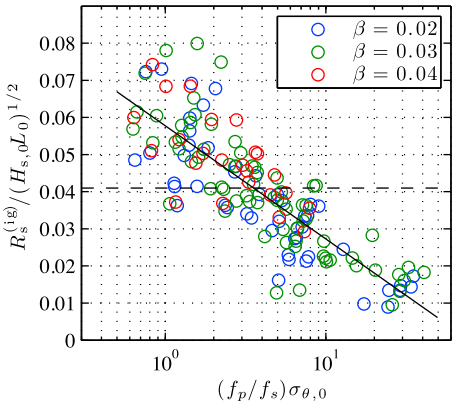

Figure 4. Normalized infragravity-band significant runup $R_s^{(ig)}/(H_{s,0}L_0)^{1/2}$ versus the nondimensional spreading parameter $(f_p / f_s)\sigma_{\theta,0}$, where $\sigma_{\theta,0}$ is the deep-water directional spread in radians. Squared correlation $r^2 = 0.69$. Colors indicate beach slope β (see legend). The horizontal dashed line is the best-fit slope 0.041 from Figure 2c. The number of simulations at each β differ.

β (lack of color banding in Figure 3b. Only $R_s^{(ig)}/(H_{s,0}L_0)^{1/2}$ depends strongly on spread, as the normalized ratio $\bar{R}/[\beta(H_{s,0}L_0)^{1/2}]$ and $R_s^{(ss)}/[\beta(H_{s,0}L_0)^{1/2}]$ have no trend with f_s and σ_θ (not shown).

4. Discussion: Parameterizing $R_s^{(ig)}/(H_{s,0}L_0)^{1/2}$

[14] The separate f_s and σ_θ dependence of $R_s^{(ig)}/(H_{s,0}L_0)^{1/2}$ (Figure 3) is shown to collapse with a single non-dimensional variable. In shallow and constant depth, two approximately co-linear incident waves with slightly different frequencies Δf are in near-resonance with the infragravity wave of frequency Δf, resulting in infragravity wave growth [*Herbers and Burton*, 1997]. In intermediate and deep water, this nonlinear interaction forces a small, second order bound infragravity wave at Δf [*Longuet-Higgins and Stewart*, 1962]. The bound wave solution is singular at the shoreline. However, in the limit of small but finite depth, small beach slope, and weak nonlinearity, the steady near-resonant and bound infragravity wave solutions are equal [*Herbers and Burton*, 1997]. Although infragravity-band runup may be dominated by resonantly forced waves, this equality motivates use of the bound-wave formalism to guide parameterizing the dependence of $R_s^{(ig)}/(H_{s,0}L_0)^{1/2}$ on f_s and σ_θ.

[15] The bound total infragravity energy E_{IG} in shallow depth h is elated to the (linearly unshoaled on plane parallel contours) deep-water sea-swell frequency directional spectrum $E(f, \theta)$ via [*Herbers et al.*, 1995]

$$E_{IG} = \int_{f\min}^{f\max} df_1 \int_{f_1+\Delta f\min}^{f_1+\Delta f\max} df_2 \int_{-\pi}^{\pi} d\theta_1 \int_{-\pi}^{\pi} \cdot d\theta_2 \left[h^{-5} C^2(f_1, f_2, \theta_1, \theta_2) E_0(f_1, \theta_1) E_0(f_2, \theta_2)\right] \quad (2)$$

where $(f_{\min}, f_{\max})$ and $(\Delta f_{\min}, \Delta f_{\max})$ are the frequency ranges of the swell and infragravity waves, respectively), and C^2 is a coupling coefficient. The bound-wave expression (2), used to model the observed directional properties of free infragravity waves [*Herbers et al.*, 1995], was later shown to be related to resonant free infragravity waves [*Herbers and Burton*, 1997]. C^2 is maximum for the special, well-studied case of a wave-flume; normal wave incidence with zero directional spread. In this case C^2 depends weakly on Δf (where $\Delta f = f_2 - f_1$) [e.g., *Sand*, 1982]. However, for directionally spread waves, C^2 is sensitive to both $\Delta\theta = \theta_2 - \theta_1$ and Δf [*Sand*, 1982]. For small angles and narrow-banded waves,

$$C^2(f_p, \Delta f, \Delta\theta) \propto \left\{1 + \left(\frac{\Delta\theta f_p}{\Delta f}\right)^2\right\}^{-2} \quad (3)$$

where $\Delta\theta \ll 1$ and $\Delta f/f_p \ll 1$. Note that $\Delta\theta f_p/\Delta f$ need not be small. With an artificial top-hat $E_0(f, \theta)$ with frequency width f_s and deep-water directional width $\sigma_{\theta,0}$, integration of (2) with (3) results in E_{IG} that depends strongly on $(f_p / f_s)\sigma_{\theta,0}$, where deep water $\sigma_{\theta,0} = (c_0/c)\sigma_\theta$ [*Herbers et al.*, 1999] and c_0 and c are the deep-water and constant-depth region phase speeds at f_p. The modeled $R_s^{(ig)}/(H_{s,0}L_0)^{1/2}$ decreases with decreasing f_p and increasing σ_θ (Figure 3), consistent with (3). In the limit of $f_s \to 0$, a monochromatic wave, infragravity wave energy is zero (3), consistent with the trend in the modeled $R_s^{(ig)}/(H_{s,0}L_0)^{1/2}$ (Figure 3a). This motivates examining the normalized infragravity runup $R_s^{(ig)}/(H_{s,0}L_0)^{1/2}$ dependence on $(f_p/f_s)\sigma_{\theta,0}$. For all simulations, $R_s^{(ig)}/(H_{s,0}L_0)^{1/2}$ variation is well parameterized (skill $r^2 = 0.69$) using $(f_p/f_s)\sigma_{\theta,0}$ (Figure 4). The best-fit relationship is

$$R_s^{(ig)}/(H_{s,0}L_0)^{1/2} = -0.013\ln\left[(f_p/f_s)\sigma_{\theta,0}\right] + 0.058. \quad (4)$$

Over the range $0.6 < (f_p/f_s)\sigma_{\theta,0} < 30$, $R_s^{(ig)}/(H_{s,0}L_0)^{1/2}$ varies a factor of 4. A similar relationship holds (although with smaller $r^2 = 0.54$) using σ_θ. As before (Figure 3b), $R_s^{(ig)}/(H_{s,0}L_0)^{1/2}$ does not depend systematically on β over the limited range considered (symbol colors in Figure 4). Modifying the $R_s^{(ig)}$ parameterization from using only $(H_{s,0}L_0)^{1/2}$ ($r^2 = 0.67$, Figure 2a) to also include $(f_p / f_s)\sigma_{\theta,0}$(4) improves the skill ($r^2 = 0.80$). This suggests a new $R_s^{(ig)}$ parameterization that may improve predictions of coastal flooding and erosion risk.

5. Summary

[16] The Boussinesq wave model funwaveC is used to simulate shoreline setup and runup over a range of incident significant wave height, peak period, frequency and directional spread, and beach slope. The model uses a simple planar beach with idealized incident wave spectra. Wave runup is simulated with a "thin-layer" method. The model reproduces the existing empirical parameterizations for setup and runup based on $(H_{s,0}L_0)^{1/2}$ or $\beta(H_{s,0}L_0)^{1/2}$. The focus here is understanding infragravity runup, which in energetic conditions dominates the sea-swell runup. The normalized runup $R_s^{(ig)}/(H_{s,0}L_0)^{1/2}$ is shown to depend on frequency (f_s) and directional (σ_θ) spread of the incident wave spectrum. Motivated by a simple analysis of near-resonant infragravity waves, the scatter about the $R_s^{(ig)}/(H_{s,0}L_0)^{1/2}$ parameterization is collapsed by a single non-dimensional variable $(f_p/f_s)\sigma_{\theta,0}$ ($\sigma_{\theta,0}$ is the deep-water directional spread). Although the model incident wave field and bathymetry are idealized, the results suggest that including $(f_p / f_s)\sigma_{\theta,0}$ in parameterizations

could improve predictions of infragravity runup and coastal flooding during energetic wave events.

Appendix A: Sensitivity to Model Domain and Offshore Sponge Layer Size

[17] The sensitivity of $R_s^{(ig)}$ to variations in model geometry (alongshore and cross-shore domain size, and offshore sponge layer width) was examined with a subset of simulations. Reducing L_y by 40% resulted in small (<10%) changes in $R_s^{(ig)}$, much less than the variation of $R_s^{(ig)}/(H_{s,0}L_0)^{1/2}$ associated with f_s and σ_θ. Results with the 70 to 100-m wide sponge layer (used in the simulations, the base case, Figure 1) were compared with results from simulations with a 700 m wide sponge layer and with an additional 600-m long constant depth domain before the 100-m wide sponge layer. Relative to the base case, the 700-m long sponge layer simulations reduced infragravity energy reflection at the offshore model boundary, and the 600-m longer domain simulations altered the tank mode frequencies. Although the infragravity runup spectra varied with different cross-shore domain and sponge layer configurations, the normalized $R_s^{(ig)}/(H_{s,0}L_0)^{1/2}$ varied by <10%.

[18] **Acknowledgments.** Support was provided by US Army Corps of Engineers, the California Department of Boating and Waterways, and NSF. This study was conduced in collaboration with SPAWAR Systems Center Pacific under grant SI-1703 from the Strategic Environmental Research and Development Program (SERDP). The authors contributed equally to this work.

[19] The Editor thanks two anonymous reviewers for assisting in the evaluation of this paper.

References

Anselme, B., P. Durand, Y. F. Thomas, and A. Nicolae-Lerma (2011), Storm extreme levels and coastal flood hazards: A parametric approach on the French coast of Languedoc (district of Leucate), *C. R. Geosci.*, *343*, 677–690, doi:10.1016/j.crte.2011.07.006.

Carrier, G. F., and H. P. Greenspan (1958), Water waves of finite amplitude on a sloping beach, *J. Fluid Mech.*, *4*, 97–109.

Clark, D. B., F. Feddersen, and R. T. Guza (2011), Modeling surf zone tracer plumes: 2. Transport and dispersion, *J. Geophys. Res.*, *116*, C11028, doi:10.1029/2011JC007211.

Feddersen, F., D. B. Clark, and R. T. Guza (2011), Modeling surf zone tracer plumes: 1. Waves, mean currents, and low-frequency eddies, *J. Geophys. Res.*, *116*, C11027, doi:10.1029/2011JC007210.

Guza, R. T., and E. B. Thornton (1982), Swash Oscillations on a Natural Beach, *J. Geophys. Res.*, *87*, 483–491, doi:10.1029/JC087iC01p00483.

Herbers, T. H. C., and M. C. Burton (1997), Nonlinear shoaling of directionally spread waves on a beach, *J. Geophys. Res.*, *102*, 21,101–21,114.

Herbers, T. H. C., S. Elgar, and R. T. Guza (1995), Generation and propagation of infragravity waves, *J. Geophys. Res.*, *100*, 24,863–24,872.

Herbers, T. H. C., S. Elgar, and R. T. Guza (1999), Directional spreading of waves in the nearshore, *J. Geophys. Res.*, *104*, 7683–7693.

Holland, K. T., B. Raubenheimer, R. T. Guza, and R. A. Holman (1995), Runup kinematics on a natural beach, *J. Geophys. Res.*, *100*(C3), 4985–4993.

Holman, R. A. (1986), Extreme value statistics for wave run-up on a natural beach, *Coastal Eng.*, *9*, 527–544.

Kuik, A. J., G. P. V. Vledder, and L. H. Holthuijsen (1988), A method for the routine analysis of pitch-and-roll buoy wave data, *J. Phys. Oceangr.*, *18*, 1020–1034.

Longuet-Higgins, M., and R. Stewart (1962), Radiation stress and mass transport in gravity waves, with application to "surf beats," *J. Fluid Mech*, *13*, 481–504.

Lynett, P. (2006), Nearshore modeling using high-order Boussinesq equations, *J. Waterw. Port Coastal Ocean Eng.*, *132*, 348–357.

Nwogu, O. (1993), Alternative form of Boussinesq equations for nearshore wave propagation, *J. Waterw. Port Coastal Ocean Eng.*, *119*, 618–638.

Puleo, J. A., and K. T. Holland (2001), Estimating swash zone friction coefficients on a sandy beach, *Coastal Eng.*, *43*, 25–40.

Raubenheimer, B., and R. T. Guza (1996), Observations and predictions of run-up, *J. Geophys. Res.*, *101*, 25,575–25,587.

Revell, D. L., R. Battalio, B. Spear, P. Ruggiero, and J. Vandever (2011), A methodology for predicting future coastal hazards due to sea-level rise on the California Coast, *Clim. Change*, *109*, 1–26, doi:10.1007/s10584-011-0315-2.

Ruessink, B. G., M. G. Kleinhans, and P. G. L. van den Beukel (1998), Observations of swash under highly dissipative conditions, *J. Geophys. Res.*, *103*(C2), 3111–3118, doi:10.1029/97JC02791.

Ruggiero, P., P. D. Komar, J. J. Marra, W. G. McDougal, and R. A. Beach (2001), Wave runup, extreme water levels and the erosion of properties backing beaches, *J. Coastal Res.*, *17*, 407–419.

Salmon, R. (2002), Numerical solution of the two-layer shallow water equations with bottom topography, *J. Mar. Res.*, *60*, 605–638.

Sand, S. E. (1982), Long waves in directional seas, *Coastal Eng.*, *6*, 195–208.

Senechal, N., G. Coco, K. R. Bryan, and R. A. Holman (2011), Wave runup during extreme storm conditions, *J. Geophys. Res.*, *116*, C07032, doi:10.1029/2010JC006819.

Spydell, M. S., and F. Feddersen (2009), Lagrangian drifter dispersion in the surf zone: Directionally spread, normally incident waves, *J. Phys. Oceangr.*, *39*, 809–830.

Stockdon, H. F., R. A. Holman, P. A. Howd, and A. H. Sallenger Jr. (2006), Empirical parameterization of setup, swash and runup, *Coastal Eng.*, *53*, 573–588, doi:10.1016/j.coastaleng.2005.12.005.

Wei, G., J. T. Kirby, and A. Sinha (1999), Generation of waves in Boussinesq models using a source function method, *Coastal Eng.*, *36*, 271–299.